Measurements of Snow Crystal Growth Dynamics in a Free-fall Convection Chamber

Kenneth G. Libbrecht[1], Helen C. Morrison, and Benjamin Faber
Department of Physics, California Institute of Technology
Pasadena, California 91125

Abstract. We present a series of experiments investigating the growth of ice crystals from water vapor in the presence of a background gas. We measured growth dynamics at temperatures ranging from -2 C to -25 C, at supersaturations between 0.5 and 30 percent, and with background gases of nitrogen, argon, and air at a pressure of one bar. We compared our data with numerical models of diffusion-limited growth based on cellular automata to extract surface growth parameters at different temperatures and supersaturations. These data represent a first step toward obtaining precision ice growth measurements as a function of temperature, supersaturation, background gas pressure and gas constituents. From these investigations we hope to better understand the surface molecular dynamics that determine crystal growth rates and growth morphologies.

1 Introduction

The formation of complex structures during solidification often results from a subtle interplay of nonequilibrium, nonlinear processes, for which seemingly small changes in molecular dynamics at the nanoscale can produce large morphological changes at all scales. One popular example of this phenomenon is the formation of snow crystals, which are ice crystals that grow from water vapor in an inert background gas. Although this is a relatively simple physical system, snow crystals display a remarkable variety of columnar and plate-like forms, and much of the phenomenology of their growth remains poorly understood [1].

Recent experimental and theoretical work suggests that surface impurities play an essential role in determining snow crystal growth rates and morphologies under normal atmospheric conditions [2]. To investigate this further we need precision measurements of snow crystal growth dynamics over a range of conditions, especially as a function of impurity type and concentration within a background gas. We have constructed a free-fall convection chamber for making such measurements [3], and we describe here our first data using this apparatus. The data were mainly taken in ordinary laboratory air at a pressure of one bar and over a range of temperatures and supersaturations. We began our experiments with these conditions in order to establish a baseline of growth measurements which can be used to determine optimal experimental strategies for investigating ice growth in the presence of different impurities.

There have been a number of previous measurements of ice crystal growth under similar conditions [4, 5, 6, 7, 8], but the measurements presented here are a substantial improvement in terms of scope and overall precision. To date there have been essentially no systematic investigations of the effects of surface impurities on ice growth dynamics.

2 Observations and Modeling

Our experiments were performed in an ice crystal growth chamber that we described in [3]. The chamber was chilled to a desired temperature and filled with a background gas at a pressure of one bar. We used a heated reservoir filled with deionized water inside the chamber to produce a known water vapor supersaturation via evaporation and convective mixing. A number of crystals were nucleated and allowed to grow for several minutes while in free-fall inside the chamber. As these crystals fell (or were carried by convective currents) to a substrate at the bottom of the

[1] kgl@caltech.edu. For the latest version of this and related papers, see http://www.its.caltech.edu/~atomic/publist/kglpub.htm

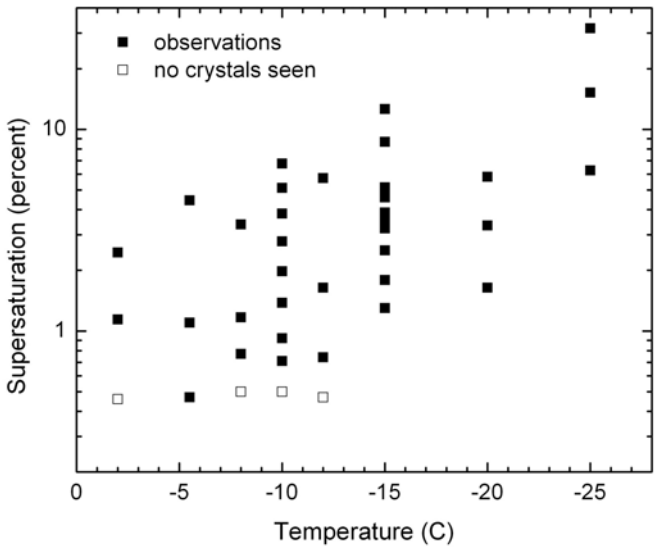

Figure 1. Graphical summary of the different temperatures and supersaturations at which we made ice crystal growth measurements for the results presented here. Open symbols show conditions at which we were unable to grow crystals.

chamber, we measured their size and thickness using a combination of optical imaging and broad-band interferometry [3]. From observations of a large number of crystals we obtained the average crystal dimensions as a function of growth time under conditions of known temperature and supersaturation, as well as some sense of the distribution of these quantities. Because of outgassing from the chamber walls and other sources, we expect that the background gas included a number of unknown impurities at the part-per-million level. We now believe that these impurities have a substantial effect on the ice growth dynamics [2], which we will be investigating in future experiments.

Figure 1 shows the different temperatures and supersaturations at which we made observations in ordinary laboratory air at a pressure of one bar. Before each run we cleaned the chamber by heating it to approximately 40 C and slowly replacing the air inside the chamber with new filtered air over a period of typically 20-40 hours. This gentle bake reduced solvent vapors and other impurities in the air to approximately the same density as in the outside laboratory air. For growth in other gases, the chamber was pumped out and new gas was introduced prior to data taking.

For measurements at temperatures above -15 C, we first cooled the growth chamber to -15 C for several hours before adding room-temperature water to the reservoir. Evaporation from the added water quickly coated the chamber walls with a thin layer of frost (and not supercooled droplets) to provide well-known boundary conditions for producing a known supersaturation inside the chamber. Following this we continuously nucleated a large number of crystals for several minutes before warming the chamber to the desired set temperature for data taking.

Most of the crystals we measured were small (< 100 μm in size) with relatively simple morphologies, and many were simple hexagonal prisms. Depending on temperature, the prism morphologies ranged from slender columns to thin plate-like crystals. Where possible we measured the plate thickness (or column length) as well as an overall crystal diameter. The latter was defined as the distance between opposing prism facets of a hexagonal prism. For the case of triangular crystals or other non-hexagonal morphologies, we used a rough estimate of the equivalent hexagonal diameter.

We write the growth velocity normal to the surface in terms of the Hertz-Knudsen formula [1]

$$v_n = \alpha v_{kin} \sigma_{surf}$$

where v_{kin} is a temperature-dependent kinetic velocity derived from statistical mechanics, σ_{surf} is the water vapor

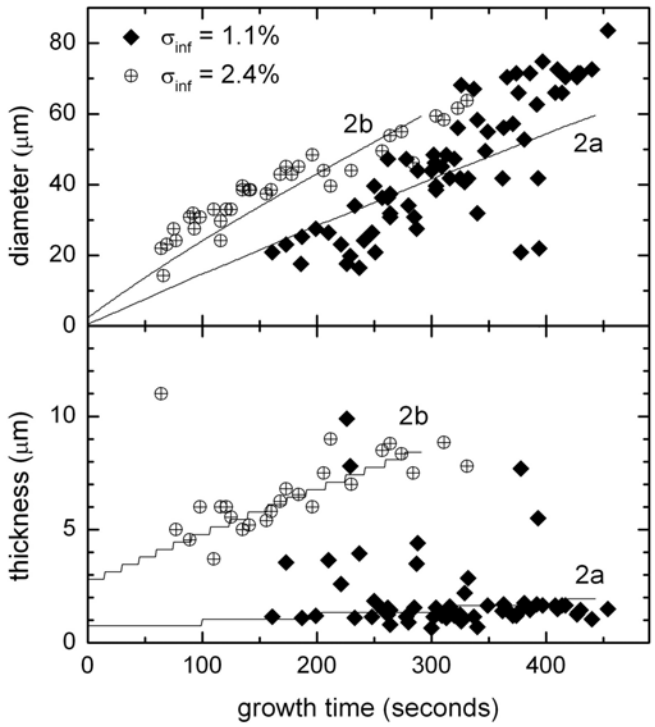

Figure 2. Ice growth data taken at -2 C at supersaturations of 1.1% and 2.4%. Each point represents the measurement of a single plate-like crystal. The labeled lines show model calculations using the parameters given in the Appendix.

supersaturation just above the growing surface, and α is the condensation coefficient, which contains the surface physics that governs how water molecules are incorporated into the ice lattice, collectively known as the attachment kinetics. If molecules striking the surface are immediately incorporated into it, then $\alpha = 1$; otherwise $\alpha \leq 1$. For ice crystals growing in an inert background gas, diffusion of water molecules to the ice surface often significantly impedes the growth [1], so that $\sigma_{surf} < \sigma_{\infty}$.

We used cellular automata to numerically model our data [9, 10] in order to extract α values from the measurements. We used a 2D approximation in which a hexagonal prism is approximated by a simple right cylinder, so the six prism facets are replaced by a single cylindrical "facet" [9]. We assumed constant values of α_{basal} and α_{prism} (i.e., with no dependence on σ_{surf}) that were adjusted so that the crystal dimensions as a function of time matched our measurements. The initial crystals in our models were typically small spheres of input diameter D_0. The initial shape was usually unimportant, however, since the model crystals always grew out into faceted shapes in a short time. For the small crystals measured, the morphologies were relatively simple and σ_{surf} was found to be fairly close to σ_{∞}. Thus we expect that modeling uncertainties in our extracted α_{basal} and α_{prism} values were relatively small. We believe that the most significant uncertainty in our current investigations stems from the unknown levels of impurities in the background gas, a topic we intend to investigate at length in future experiments.

Surface tension effects may have played some role in our measurements, but only at the lowest supersaturations. The equilibrium vapor pressure above a static spherical crystal is approximately

$$c_{eq} \approx c_{sat}\left(1 + \frac{2\delta}{R}\right)$$

where c_{sat} is the equilibrium vapor pressure above a flat surface, $\delta \approx 1$ nm is a surface tension term [1] and R is the crystal radius. From this we see that the supersaturation $\sigma = (c - c_{sat})/c_{sat}$ must be greater than $\sigma_{\min} \approx 2\delta/R$ for growth to occur. Put another way, the crystal size must be greater than $2R_{\min} \approx 4\delta/\sigma_{surf}$ or a crystal will not grow. In some cases presented below we observed σ_{surf} as low as 0.5 percent, implying $2R_{\min} \approx 0.8$ μm. Although

we sometimes observed crystals of approximately this thickness at low supersaturations, in most cases the surface tension term was negligible. Thus we did not include surface tension effects in our numerical models.

3 Results

Unless noted otherwise, the data presented in this section are from crystals grown in a background of ordinary laboratory air at a pressure of one bar. For some runs we evacuated the chamber several times while cold and filled it to one bar with bottled nitrogen or argon gas, but noticed no change in the crystal morphologies or growth rates. The temperature and supersaturation inside the growth chamber were determined as described in [3]. We used either nitrogen or argon gas for nucleation, as we observed that both gases yielded indistinguishable results.

3.1 T = -2 C

Figure 2 shows data taken at -2 C. About 90% of the crystals observed were plate-like, with the remainder being columnar or irregularly shaped crystals. In the figure we have included only well-formed plate-like crystals. Triangular plates (see [11] for example pictures) were especially common at -2 C, accounting for approximately 15% of measured crystals at $\sigma_\infty = 1.1\%$ and 7% at $\sigma_\infty = 2.4\%$. Lines in the figure show model calculations with input parameters given in the Appendix.

At 1.1%, note that the crystal diameters increase with time more rapidly than the model would suggest at the later times, and that the thicknesses do not increase substantially with time. We believe some of this behavior may be due to a systematic sampling effect. We observed crystals as they fell onto our substrate, and crystals with the highest air resistance would tend to remain aloft for the longest time inside the chamber. This factor may account for the preponderance of especially large, thin plates seen at later times in Figure 2. Note this systematic sampling error affects our data most strongly at later times after most crystals have already fallen.

3.2 T = -5.5 C

Figure 3 shows a test we performed at -5.5 C to look at systematic effects from competition between growing crystals. If a large number of crystals are nucleated inside the chamber at one time, their growth lowers the supersaturation and reduces the final sizes of the crystals. As a practice we decreased the nucleation pressure to within 1-2 psi of the minimum pressure required to produce crystals. We believe this resulted in a sufficiently small number of crystals that systematic effects in the measured crystal sizes from water vapor competition were less than 20%.

Figure 4 shows data taken at -5.5 C along with model calculations. Crystals observed at $\sigma_\infty = 4.4\%$ were typically more structured than at lower supersaturations, with hollow basal surfaces at later times. Our measurements refer to overall crystal sizes, not including hollows. Generally less structure was seen in our numerically modeled crystals. The current data are in reasonable agreement with Libbrecht and Yu [8], although in Figure 4 we show all crystals observed, not just the largest ones, so the sizes here are somewhat smaller than in [8].

In Figure 4 we see that the initial column diameter (at $t = 0$ in the model calculations) appears to increase with increasing supersaturation. The origin of this is unknown at present, but we see similar trends in much of the data presented here, particularly at temperatures between -5.5 C and -10 C. It seems unlikely that nucleation dynamics are responsible for this effect, and we suspect that the crystal growth is especially fast at early times, indicating that α is initially large and then is reduced to some nearly constant value after a short period of time. The buildup of surface impurities on an initially clean crystal may be responsible for this behavior.

3.3 T = -8 C

This temperature is midway between the growth of plate-like and columnar crystals [1], so we see much morphological diversity in the crystals, shown in Figure 5 as a broad distribution of aspect ratios $A = thickness/diameter$. In this figure we ignored a small number of blocky crystals and other poorly formed crystals. Since the majority of the

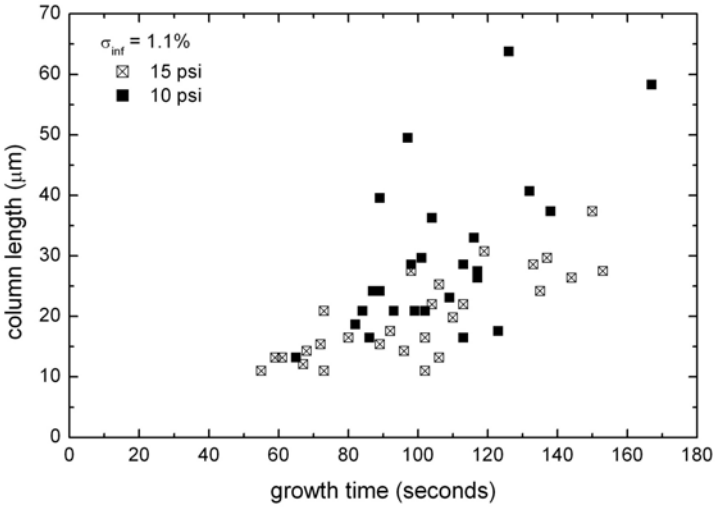

Figure 3. A comparison of crystals produced at -5.5 C using two different nucleation pressures (see [3]). The higher pressure yielded more crystals, which then competed for the available water vapor in the chamber and did not grow as rapidly.

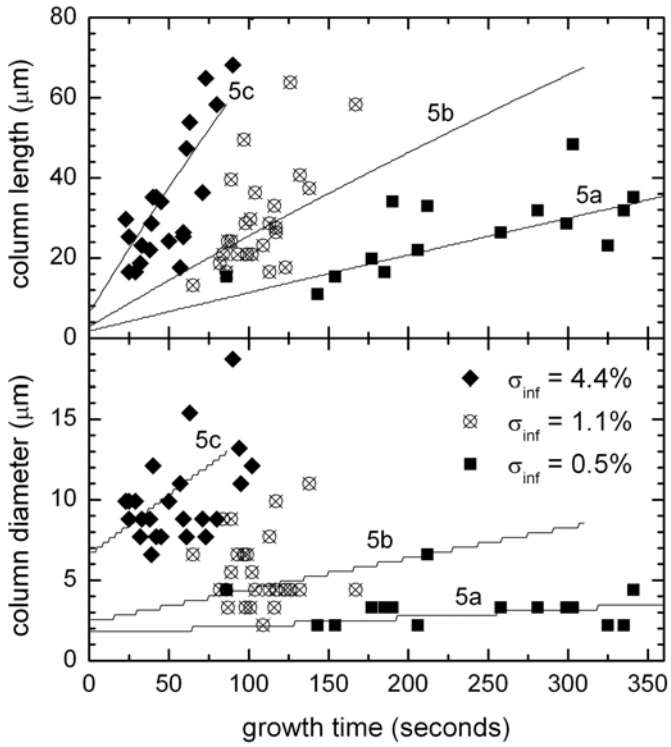

Figure 4. Ice growth data taken at -5.5 C and several different supersaturations, along with model calculations using the parameters in the Appendix.

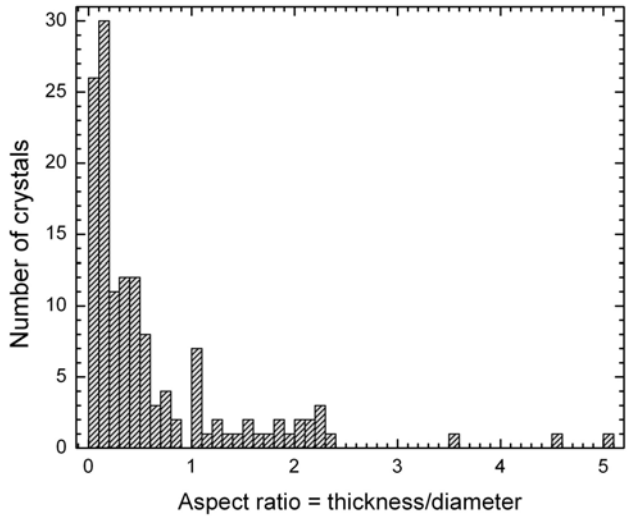

Figure 5. Distribution of aspect ratios of crystals grown at -8 C, showing a range from plates to columns.

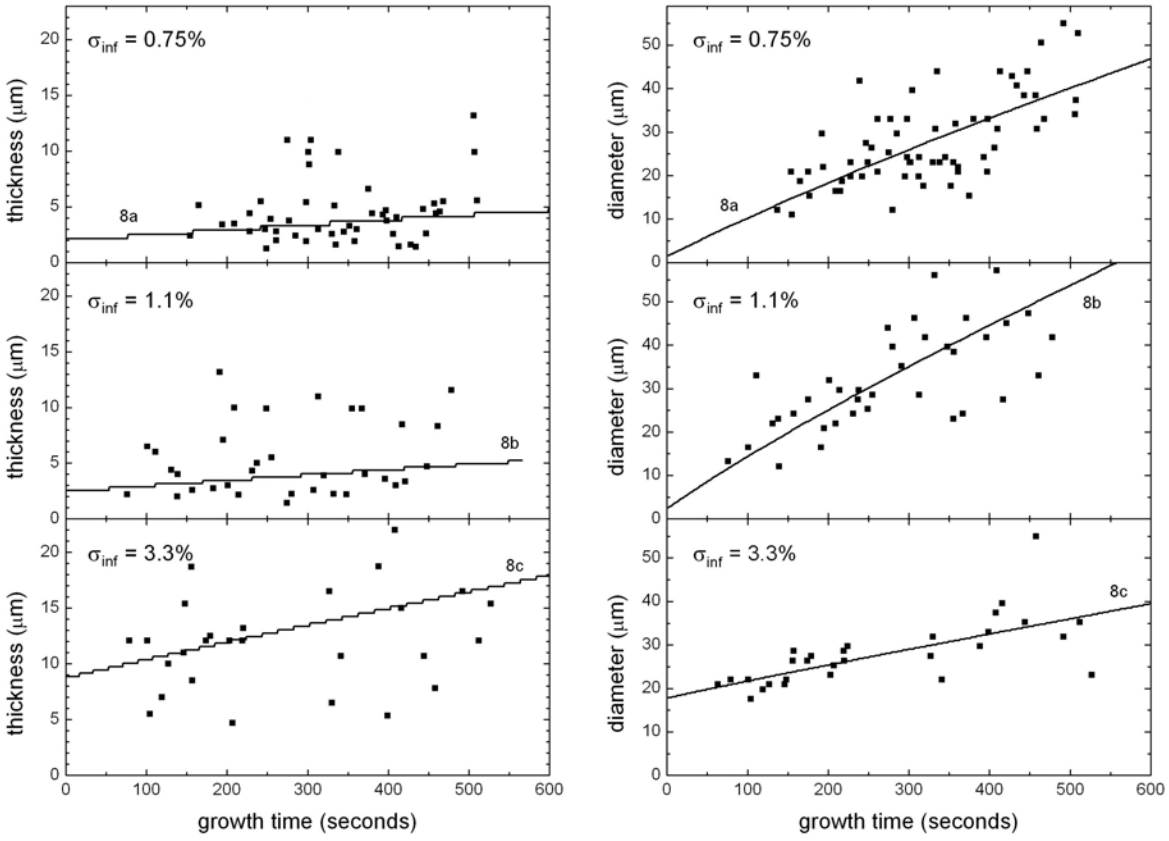

Figure 6. Data from plate-like crystals grown at -8 C, with aspect ratios less than 0.8, along with model calculations.

observed crystals were plate-like, we removed all crystals with aspect ratios greater than 0.8 (nearly half) to produce the data shown in Figure 6. In this figure, approximately 25% of the plates at $\sigma_\infty = 0.75\%$ were too thick or too structured to obtain thickness measurements, while roughly 7% could not be measured at the higher supersaturations.

In Figure 6 we again see a large initial crystal thickness when the supersaturation is high. The thicker crystals require more mass to increase the diameter D, with the result that dD/dt is highest at the intermediate supersaturation of 1.1%. From the model parameters in the Appendix, we see that the main change with supersaturation is the initial crystal diameter D_0.

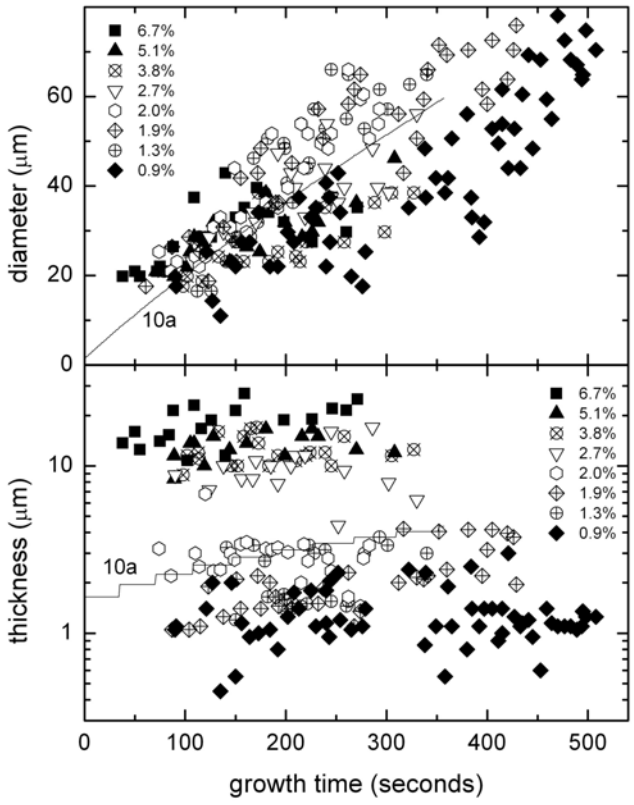

Figure 7. Data taken at -10 C over a range of supersaturations. Note the clear jump in thickness around $\sigma_\infty = 2.5\%$, and that in all cases the thicknesses are nearly constant with time.

3.4 T = -10 C

At this temperature we took data over a range of supersaturations to examine the plate thickness as a function of σ_∞, yielding the data in Figure 7. Not shown are data taken at 0.7%, which yielded essentially all small blocky crystals. At 0.9% we observed a bimodal distribution with approximately 20% blocks (with $0.1 < A < 1$) and 80% thin plates (with $A < 0.1$). The plate fraction increased at higher supersaturations. Over 80% of the plates had measurable thicknesses, with no discernible trends in this percentage with σ_∞.

The -10 C data show the rapid initial growth most clearly, and a distinct jump in the thickness data can be seen in Figure 7. Note also that the crystal thickness assumes its nearly constant later value in less than 50 seconds for the highest supersaturations. Clearly data at shorter times would be beneficial, and could be acquired by using air currents to drive crystals quickly onto the substrate. The crystals sizes at 200 seconds are shown in Figure 8. Again the thickness shows a rather abrupt jump around $\sigma_\infty = 2.5\%$. We also see a decrease in the diameter above $\sigma_\infty = 2.5\%$, which is explained simply by the jump in thickness, since a thicker crystal requires more mass for a given diameter.

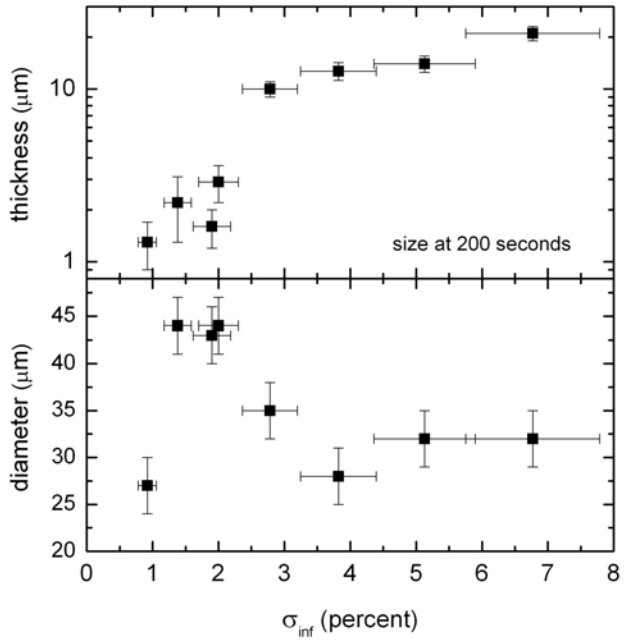

Figure 8. Crystal sizes after a growth time of 200 seconds at -10 C. Note the abrupt jump in thickness at $\sigma_\infty = 2.5\%$, which is accompanied by a decrease in crystal diameter.

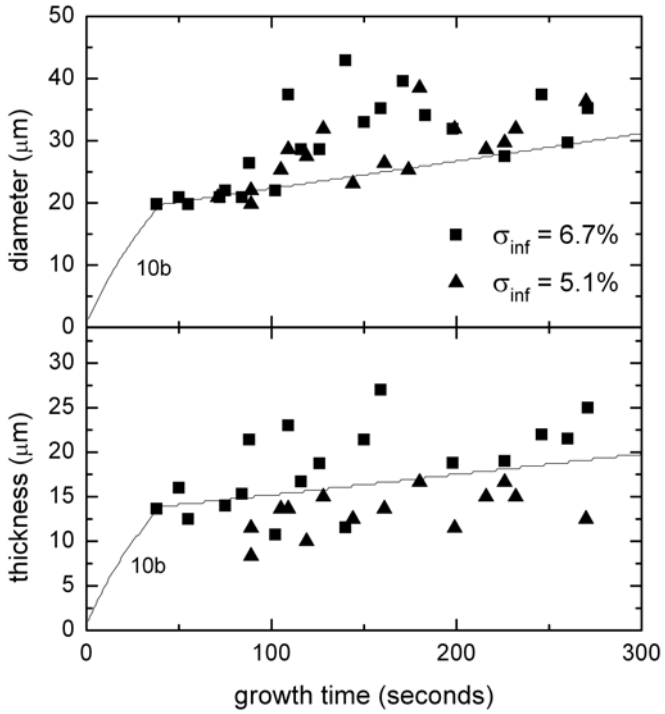

Figure 9. Data at -10 C for the highest supersaturations measured, along with model calculations described in the text.

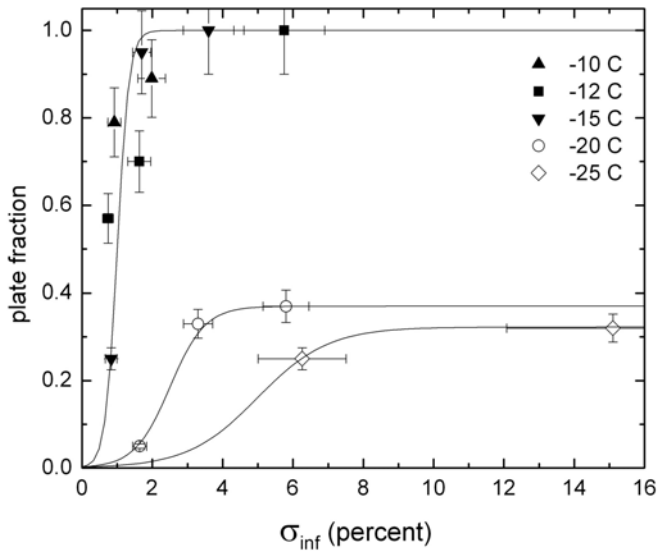

Figure 10. Fraction of crystals that were plate-like for different temperatures, as a function of supersaturation. Lines were drawn to guide the eye.

Figure 9 shows the same data at only the highest supersaturations along with a model calculation in which we assumed one set of values for α_{basal} and α_{prism} before 40 seconds and a different set after this time, as listed in the Appendix. These data suggest that both α_{basal} and α_{prism} decreased with time as the crystals grew, although other possible explanations have not been definitely ruled out.

3.5 T = -12 C

The crystals at this temperature showed a rather clear transition from blocky to plate-like morphologies with increasing supersaturation. At $\sigma_\infty = 0.4\%$ we observed no crystals, at 0.7% about 40% were blocky and the rest were plates, at 1.6% about 30% were blocks, and at 5.7% essentially all were plates. Figure 10 shows the trend as a function of σ_∞ for this and other temperatures. The precise morphologies of the blocky crystals were difficult to determine since their sizes were quite small and their aspect ratios were close to unity.

Figure 11 shows data at 1.6% that includes both plates and blocks. The blocky crystals are reasonably well described with radii that go as $R \sim t^{1/2}$. Since $\alpha \ll \alpha_{diff}$ for these crystals [1], this model implies $\alpha \sim R^{-1}$, again suggesting that α decreases with growth time even though σ_{surf} remains nearly constant. Figure 12 shows additional data for plates grown at -12 C. The plates at this supersaturation exhibited an exceedingly small α_{basal} (see the Appendix).

3.6 T = -15 C

Figure 13 shows data taken at -15 C over a range of supersaturations. The complexity of the crystals changed substantially with supersaturation at this temperature. We observed predominantly simple plates below $\sigma_\infty = 3.5\%$, more structured plates at 5.1%, simple branched plates at 8.6%, and complex branched plates at 12%. The structure in the crystals meant that the basal surfaces were often not flat enough to allow interferometric thickness measurements, as shown in Figure 14. Crystals at this temperature exhibited a marked increase in thickness with increasing σ_∞, although with a somewhat different character than at -10 C. Unfortunately, the structure in the crystals at -15 C did not allow accurate thickness measurements at high supersaturations. This temperature also produced the highest α_{prism} values, consistent with expectations from the morphology diagram.

We also examined growth in nitrogen and argon gases at -15 C and a pressure of one bar, yielding the data in

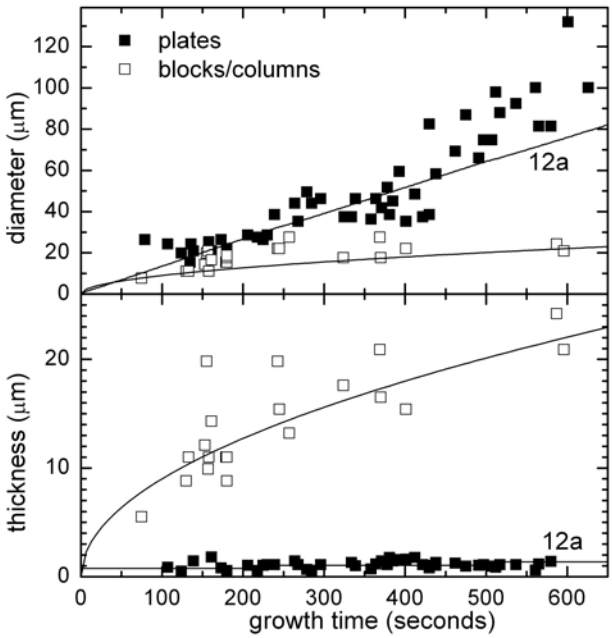

Figure 11. Data taken at -12 C and $\sigma_\infty = 1.6\%$, along with model calculations.

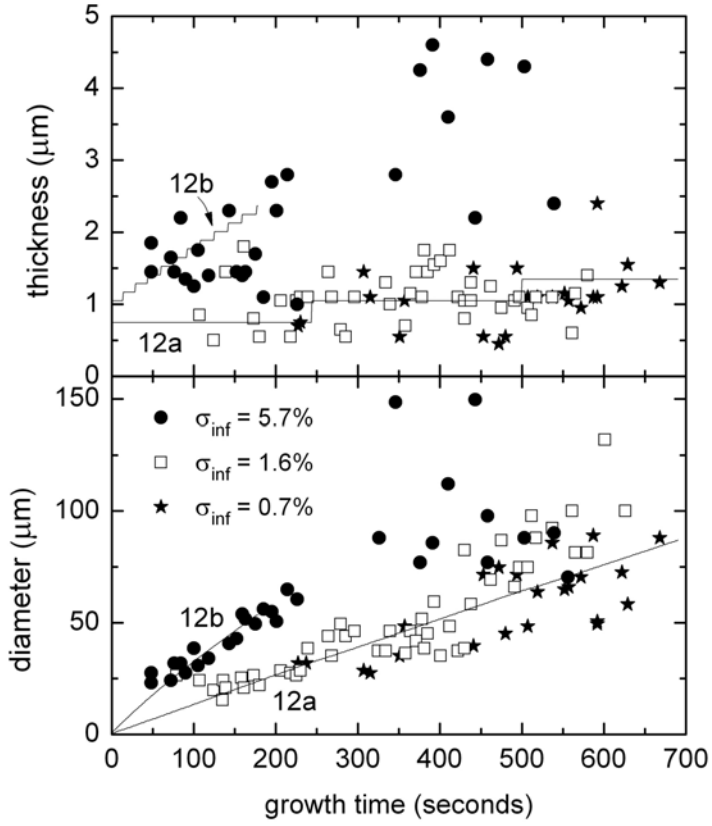

Figure 12. Data taken at -12 C, along with model calculations.

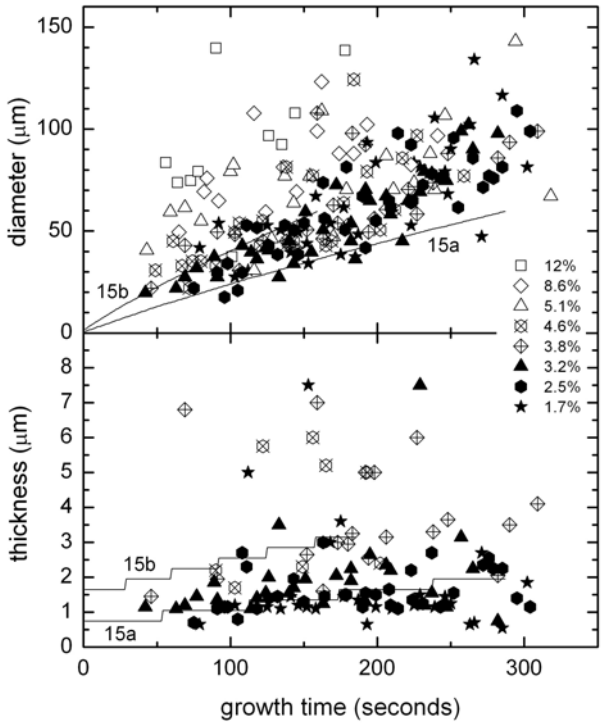

Figure 13. Data taken at -15 C and a variety of supersaturations, along with two representative models.

Figure 15. These data suggest that nitrogen and argon are equally inert in regards to their effect on ice crystal growth. A comparison with growth in air (Figure 13) further suggests that oxygen is also equally inert.

3.7 T = -20 C

We again observed a bimodal distribution of blocky and plate-like crystals at -20 C. There were few plates at $\sigma_\infty = 1.6\%$, but more at higher supersaturations, as shown in Figure 10. Growth at 5.8% is shown in Figure 16 along with model calculations.

3.8 T = -25 C

We did just a few runs at -25 C, and these did not produce much quality data. At $\sigma_\infty = 6\%$ the crystals were mainly blocky in form, with diameters of about 15 μm at 200 seconds, yielding $\alpha \approx 0.008$ for both the prism and basal faces. At $\sigma_\infty = 15\%$ a good fraction of the crystals were plate-like (see Figure 10), with thicknesses of about 8 μm and diameters of about 22 μm at 200 seconds, giving $\alpha_{basal} \approx 0.002$ and $\alpha_{prism} \approx 0.005$. At $\sigma_\infty = 30\%$ the crystals were almost entirely polycrystalline forms. These data could be improved by nucleating crystals at a higher temperature and then transferring them to the growth chamber.

4 Conclusions and Future Work

As mentioned in the introduction, the data presented here should be taken as an initial, baseline set of data to be used as a jumping-off point for future experiments. At present there is little quantitative theory with which we can compare the α values we determined. The crystal morphologies we observed as a function of temperature and supersaturation were in general agreement with the known morphology diagram, as were the extracted attachment coefficients shown in Figure 17. By modeling the growth of isolated crystals, our observations are a step toward replacing the qualitative morphology diagram with more quantitative measurements of α_{basal} and α_{prism} as a function

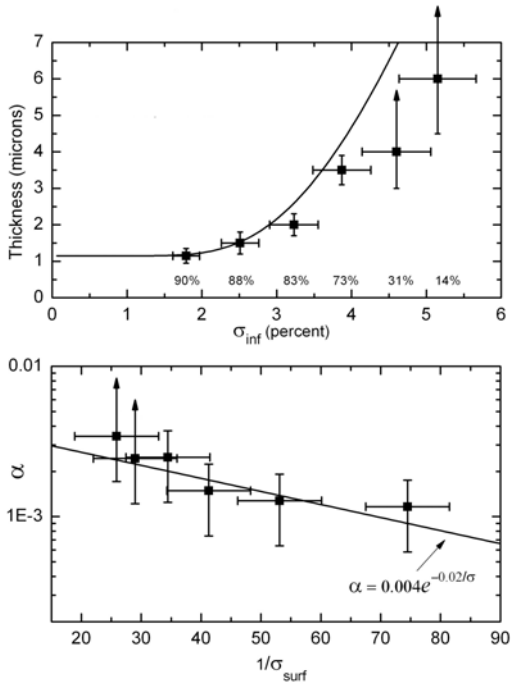

Figure 14. Top panel: Crystal thickness after 200 seconds of growth at -15 C, as a function of σ_∞. Numbers below the points give the fraction of crystals with measurable thicknesses. The line was drawn to guide the eye. Over this same range in σ_∞, the diameters at 200 seconds changed monotonically from approximately 65 to 80 μm. Lower panel: Values of the attachment coefficient α_{basal} as a function of σ_{surf}^{-1}, as determined from model calculations.

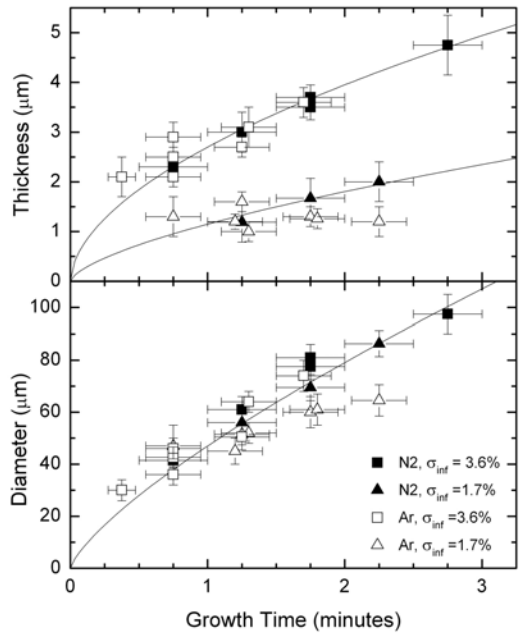

Figure 15. Comparison of crystal growth at -15 C in nitrogen and argon gas. Lines were drawn to guide the eye. These data suggest that nitrogen and argon gases are equally inert regarding their effect on ice crystal growth.

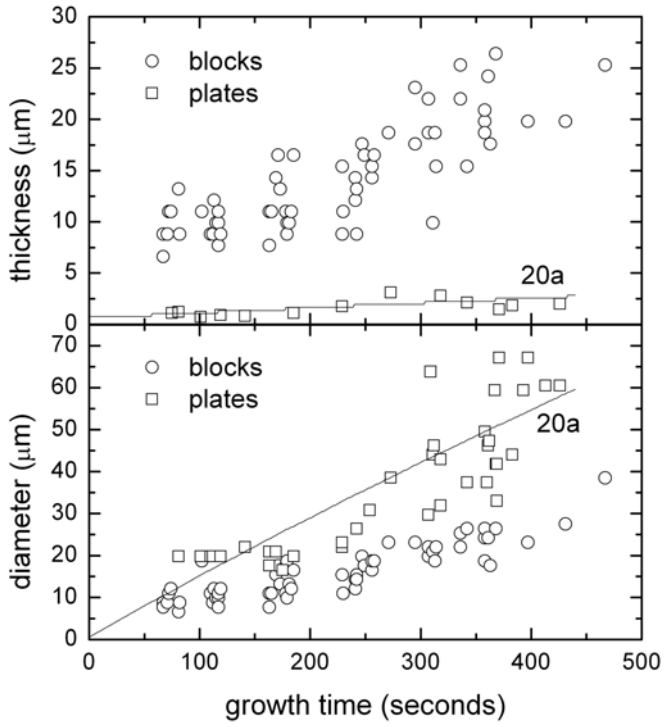

Figure 16. Growth data at -20 C and a supersaturation of $\sigma_\infty = 5.8\%$, showing both plate-like and blocky crystals.

of temperature and supersaturation.

The present measurements were made mainly in ordinary air, which contains impurities at some unknown level. We now believe that gaseous impurities play an essential role in snow crystal growth [2], which means much greater attention must be paid to the composition of the background gas. Additional experiments with gaseous impurity levels both higher and lower than we had in the current experiments would be especially interesting. The data presented here are useful for determining optimal strategies for investigating ice crystal growth in different chemical environments.

We observed a number of features in our data that should be investigated further. The fast initial growth observed at -10 C (as well as at other temperatures) may be a useful indicator of impurity effects, and this is certainly worth examining further, especially as a function of supersaturation. Statistics on the numbers of triangular plates produced, as well as other unusual plate-like morphologies, could also be pursued. A more careful examination of growth morphologies between -6 C and -10 C may also yield better insights into the transition from plate-like to columnar growth.

5 Acknowledgements

We acknowledge support for HCM and BF by the Caltech Summer Undergraduate Research Fellowship (SURF) program, the CamSURF program, and the Robert L. Blinkenberg SURF Endowment.

6 Appendix - Model Parameters

We modeled our data using the 2D cellular automata method described in [9]. We used constant input growth parameters α_{basal} and α_{prism}, along with an input initial crystal diameter D_0. These parameters were adjusted to to produce model crystals that fit our measurements. In addition to the crystal thickness and diameter as a function

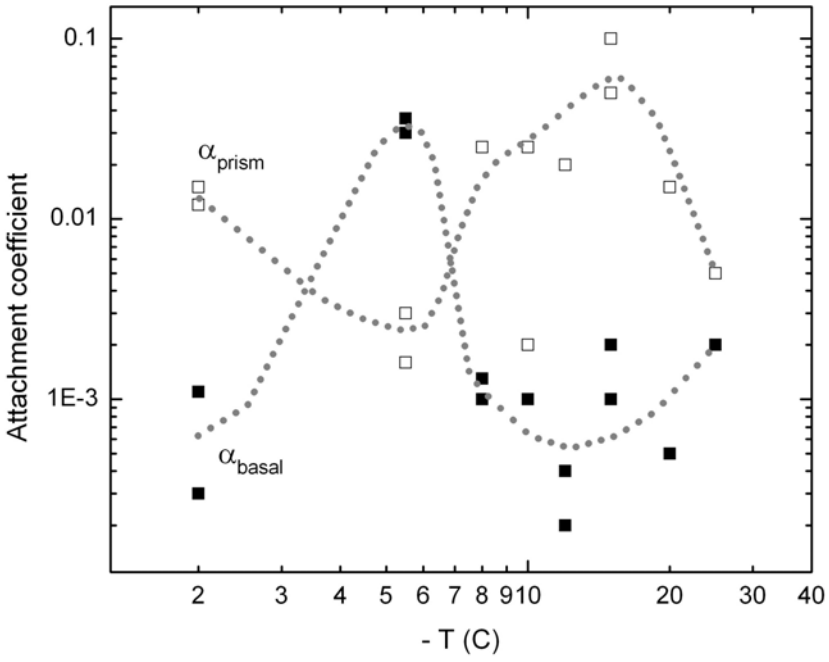

Figure 17. Summary of our measured attachment coefficients α_{basal} and α_{prism} from the Appendix, as a function of temperature. Data at all supersaturations are shown, and lines were drawn to guide the eye. The overall trends in these data agree with the well-known snow crystal morphology diagram.

of time shown in the graphs, the model also yielded σ_{surf} at all points on the crystal surface as a function of time. From these data we extracted roughly average values for σ_{surf} on the basal and prism facets, which are shown in the table. We believe that overall uncertainties in σ_∞ and the derived quantities are roughly 20% throughout, mainly from a variety of systematic errors in the measurements.

Model#	T (C)	σ_∞ (%)	α_{basal}	α_{prism}	D_0 (μm)	$\sigma_{surf,basal}$ (%)	$\sigma_{surf,prism}$ (%)
2a	-2	1.1	0.0003	0.015	1	1.0	0.9
2b	-2	2.4	0.0011	0.012	3	2.0	1.8
5a	-5.5	0.5	0.03	0.0016	2	0.4	0.45
5b	-5.5	1.1	0.036	0.003	3	0.8	0.95
5c	-5.5	4.4	0.03	0.003	7	3.0	3.5
8a	-8	0.75	0.0013	0.025	2	0.6	0.5
8b	-8	1.1	0.001	0.025	3	0.9	0.75
8c	-8	3.3	0.001	0.025	18,9	2.6	2.1
10a	-10	2	.001	.025	2	1.6	1.5
10b	-10	6	0.02,0.001	0.03,0.002	1	4.0	4.0
12a	-12	1.6	0.0002	0.02	1	1.4	1.3
12b	-12	5.7	0.0004	0.02	1	5.0	4.0
15a	-15	2	0.001	0.1	1	1.5	1.2
15b	-15	4	0.002	0.05	2	3.0	2.2
20a	-20	5.8	0.0005	0.015	1	5.2	5.0

7 References

[1] K. G. Libbrecht, "The physics of snow crystals," Rep. Prog. Phys. 68, 855-895 (2005).

[2] K. G. Libbrecht, “Crystal growth in the presence of surface melting and impurities: An explanation of snow

crystal growth morphologies," paper 0810.0689 in the arXiv.org e-Print archive (2008).

[3] K. G. Libbrecht and H. C Morrison, "A convection chamber for measuring ice crystal growth dynamics," paper 0809.4869 in the arXiv.org e-Print archive (2008).

[4] A. Yamashita, Kisho Kenkyu Noto, Meterorol. Soc. Jpn. 123, 47 (1974).

[5] T. Kobayashi, T. Kuroda, in: I. Sunagawa (ed.), Morphology of Crystals, Part B, Terra Scientific, Tokyo (1987).

[6] B. F. Ryan, E. R. Wishart, D. E. Shaw, J. Atmos. Sci. 33, 842 (1976)

[7] T. Takahasi, T. Endoh, G. Wakahama, N. Fukuta, J. Meteorol. Soc. Jpn. 69, 15 (1991).

[8] K. G. Libbrecht and H. Yu, "Crystal growth in the presence of surface melting: Supersaturation dependence of the growth of columnar ice crystals," J. Cryst. Growth 222, 822 (2001).

[9] K. G. Libbrecht, "Physically derived rules for simulating faceted crystal growth using cellular automata," paper 0807.2616 in the arXiv.org e-Print archive (2008).

[10] J. Gravner and D. Griffeath, "Modeling snow crystal growth II: A mesoscopic lattice map with plausible dynamics," Physica D 237, 385-404 (2008).

[11] K. G. Libbrecht, "Ken Libbrecht's Field Guide to Snowflakes," (St. Paul: Voyageur Press) (2006).